

Light Curve of Algol using CCD camera and C8-Telescope

Yael Demers (260904387), Aidan Lewandowski (260910544), Jessie Zhao (260890021)
McGill Physics Department

April 28, 2023

This project aims to replicate the light curve of Algol, a binary star, using data from the Transiting Exoplanet Survey Satellite (TESS) mission and our experimental observations. To achieve this, we utilized a Celestron NEXIMAGE 5 SOLAR SYSTEM IMAGER (5MP) CCD camera, a Celestron C8SE telescope, and *oaCapture* software. We collected flux data from Algol and a reference star, Capella, using aperture photometry, while dark frames were used to minimize the CCD camera and background noise. Due to altitude and observing time limitations, we used Capella's luminosity to scale Algol's flux data. Our experimental light curve of Algol was then compared to TESS' 2022 light curves, and the mean luminosity of Algol obtained from our data was $(6.0 \pm 1.1) \times 10^{28}$ W. The theoretical luminosity of Algol was $(6.97 \pm 0.08) \times 10^{28}$ W, which was within one standard deviation of our result. Furthermore, 69.4% of our data points were within TESS' light curve according to the 2/3 rule of fitting data.

Binary Systems | Light Curves | Beta Persei | Algol

servations have shown that approximately 33% of solar systems are binaries [2]. Binary systems can be further categorized into visual, spectroscopic and eclipsing. Visual binaries mean they can be seen directly in a telescope, and spectroscopic binaries mean that they can be observed from their stellar spectral lines due to Doppler shifts. Eclipsing binaries mean that they can be identified by characteristic variations in their light curve. Eclipsing binaries are the subject of study in this report. Light curves are plots that show the changes in light fluxes or luminosities with respect to time, where the flux is the amount of energy from the star that reaches the observer and luminosity is an absolute measure of light or the radiant power emitted by the star over time. Flux has a linear relationship with luminosity, the equation is as follows:

$$f = \frac{L}{4\pi r^2} \quad (1)$$

1 Introduction

The types of stars can be divided into four different categories: single stars, binary stars, triple stars and quadruple stars. Single-star systems consist of solitary stars that are not gravitationally bound to other stars, such as our Sun. On the other hand, binary star systems consist of pairs of stars and are gravitationally bound so that they are rotating in orbits around a common center of mass [1]. The stars in triple-star systems and quadruple-star systems also rotate with each system's center of mass. Single star systems are the most common configuration for solar systems seen in the Milky Way, but recent ob-

where f is the flux, L is the luminosity and r is the distance to the star. Luminosity is an intrinsic measurable property of a star independent of distance, but Flux shows how bright an object is to the observer, and is inversely proportional to the square of distance [3].

Because flux has a linear relationship with luminosity if the distance (from the star to an observer) is fixed, flux and luminosity should exhibit similar behaviours in the light curve of that star. An eclipsing binary is expected to have a light curve similar to that of Fig.1.

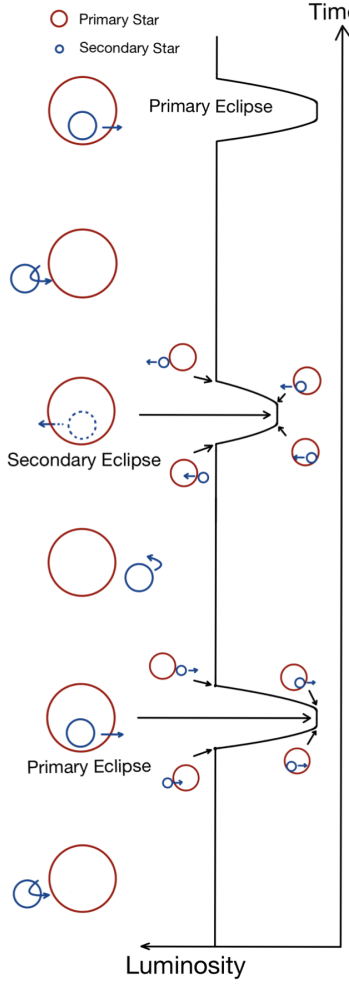


Figure 1: Eclipsing Binary. This is the process of an eclipsing binary containing a full rotation period. The red (larger) star is called the primary star and the blue (smaller) star is called the secondary star. The luminosity versus time plot is the light curve of this binary, and the stars drawing on the side are the corresponding star motions. When the secondary is blocking the primary, it is called the primary eclipse and when the primary is blocking the secondary, it is called the secondary eclipse.

Since a binary system contains two stars, the more massive one is also called the primary star (shown as red in Fig.1), while the lighter one is called the secondary (shown as blue in Fig.1). We will assume the primary star is much more massive than the secondary star so that their common center of mass is located at the primary's center. In this case, the primary star is fixed, and the secondary star is rotating around the primary star. Fig.1 also assumes that the secondary star is orbiting in a circular motion, so the motions and the light curves are symmetric. The

higher plateaus appear when neither the primary is blocking the secondary nor the secondary is blocking the primary, and the other plateaus are either when the primary is completely blocked by the secondary or the secondary is completely blocked by the primary. This is called the *transit duration*. When the secondary is orbiting in front of the primary, the light coming from the primary will be blocked by the primary, and the light curve will drop. This transit is called the primary eclipse. On the other hand, when the primary is blocking the light from the secondary, the light curve will also drop. This transit is called the secondary eclipse. However since we assumed the primary star is brighter than the secondary, when the primary is being blocked (primary eclipse), the light curve will drop to a lower point than the other transit.

Another quantity known as *apparent magnitude* is also a brightness measure of a star. It also shows how bright a star is to a specific observer, which means it is not an intrinsic property of a star. *Absolute magnitude* on the other hand, is a measure of a star's intrinsic property, and it does not depend on the location of the observer. Both apparent and absolute magnitudes are inverse logarithmic scales so that the brighter the object, the lower the value of the magnitude.

The purpose of this project is to reproduce the light curve of the binary star Algol using data from the Transiting Exoplanet Survey Satellite (TESS) mission and our experimental data. We aim to determine the luminosity of the binary system throughout a given period as well as identify any discrepancies between our experimental data and the TESS data. The repeatability of this experiment is crucial for verifying the accuracy of our results and advancing our understanding of binary star systems.

2 Experimental Methods

2.1 New Software

For this experiment, some new software was used to take the Charged Coupled Device (CCD) images. *oa-Capture* is an astronomy imaging software that was used to take the calibration images and images of our objects of interest. We learned how to use the software and extract data from it, but that will be discussed further in the report [4].

2.2 CCD Calibration

2.2.1 Mock Test Calibration

Before taking pictures of the binary system with a telescope, a calibration of the Charged Coupled Device (CCD) camera is needed. The CCD camera used in this experiment is the *Celestron NEXIMAGE 5 SOLAR SYSTEM IMAGER (5MP)* [5]. The calibration process was first done in a laboratory. This was to ensure that the images were taken correctly and acted as a trial run for the actual calibration of the CCD camera with the telescope that would be performed during observation. The process of calibrating the CCD camera involves two sets of images: dark frames and bias frames.

A dark frame is a measurement of the thermal noise caused by the telescope's surroundings during observation. The external temperature in the CCD's surroundings can affect background noise which affects the image. Thermal electrons can be confused for photoelectrons which cause a growing noise at higher temperatures. A dark frame is done by taking a one-second image exposure with the camera shutter closed. The dark frame will be at the same temperature as the image of the binary system and will have approximately the same thermal noise, thus making it possible to subtract this additional noise from the final image [6]. The CCD camera utilized in this experiment did not have a shutter that could be closed, so the mock test dark frames were taken in a dark room with no natural light, and all artificial lights off. Twenty frames were taken in total and averaged to get a final image (the averaging process will be explained later in this section).

A bias frame is used to describe a CCD camera's pixel-to-pixel variation. Each pixel has a slightly different base value, and this bias can be removed from the final image by taking a bias frame [6]. A bias frame is taken by taking a zero-second exposure (more like 0.01-0.1 second exposure since *oaCapture* software will not allow shorter). The bias frame should be taken at the same temperature as the dark frame. Like the dark frame mock test, twenty bias frames were taken. These photos were taken in regular artificial light, with 0.1-second exposures for each, and then were averaged to get a final image.

To average the frames, a Python script was created. The image files were saved in *.fits* format. A for loop was made to compile all of the data from the frames into a list and converted it into an array. Then, another for loop was used to iterate through

all of the pixels in each image (dimensions 1944 by 2592 pixels), and then take the mean of all image pixels at that [i, j] position. This would return a single image that contained the averaged pixels from the set of twenty images. This averaging method was used for both the dark frames dataset and the bias frames dataset. The calibration frame results can be seen in Appendix B.1.

2.2.2 Calibrating CCD with Telescope

Dark Frames are taken at the beginning of each observation and the end of each observation, as the external temperature may change throughout the night. To connect the CCD camera to the telescope, the diagonal mirror eyepiece was removed from the end of the telescope, and the CCD was secured onto the end with a telescope attachment. A cable was connected from the camera to the laptop that took the data. Since the CCD camera shutter did not close, the telescope cap was put onto the end of the telescope to block all of the light. Like the mock session, twenty photos were taken with one-second exposures and then averaged to get a single dark frame image. Reference frames were done by taking photos of another star, and were used to indicate how the observation changes between different stars. Dark Frames and Reference Frames were taken for each of the four observing sessions (although the unsuccessful observing session calibration frames will not be included in this report). Once it was calibrated properly, the CCD camera was ready for use.

2.3 Telescope Calibration

The telescope used in this experiment is the *Celestron C8SE*. Observations using this telescope took place on the roof of the Rutherford Physics building at the Anna McPherson Observatory. The telescope has a computerized mount feature that enables the observer to find an object of interest faster after doing some calibration. There is also a finderscope located on the top of the tube that allows for manual adjustment. When an object of interest has been located, the finderscope has a laser pointer to align the object at the center of the scope, with manual adjustments being made by the computerized mount motor. Once the object is centered in the finderscope, the eyepiece is used to center the object for recording data. There is an "X" that is used to align the object in the center of the eyepiece and is finely adjusted by using the computerized motor. The telescope components discussed can be seen in Fig.2.



Figure 2: Apparatus - Telescope Components This is the telescope utilized in this experiment. The computerized motor has multiple motor speeds that allow for large or fine adjustments. The Eyepiece is shown as the furthest right component attached to the telescope. The focal reducer (left) and finderscope (right) are the two separate objects on this diagram [7].

Star alignment is a crucial portion of the C8 telescope calibration. For observing dimmer sources (like our binary system), it is crucial to align a few other known sources before finding the source of interest. This is achieved by aligning the telescope with a known star and helps the telescope orient itself in the night sky. The desired reference star is inputted into the computerized motor, and then fine adjustments are made in both the finderscope and eyepiece. For each night of observation, a star alignment with two known stars was used to perform the calibration. Then, the star of interest was inputted into the device, and the telescope would rotate itself toward the star. Despite the calibration, the computerized motor was not completely accurate, so a finer adjustment was performed manually with the finderscope and eyepiece.

When the star of interest was aligned in the eyepiece, the eyepiece was replaced with the CCD camera, and the data was recorded by a personal laptop (see Fig.3 for experimental setup). Due to the CCD camera's zoom, some adjustments were made with the computerized motor to ensure that the star appeared in the frame for the photos on the laptop. Photos were again taken with the *oaCapture* software.



Figure 3: Apparatus - Experimental Setup When taking observations, the following components are used: a tracking computer for identifying the star system, a finderscope (eyepiece) for orienting the star in the image, a CCD camera for recording data, a connector cable, a telescope stand, and a laptop that records the data. This diagram was made using SketchUp software.

2.4 Finding Interest Binary

Due to the light pollution, the apparent magnitude of the star needed to be brighter than 4. As mentioned in Sec.1, the value of magnitude is smaller when the star is brighter. This means the star needs to have a magnitude value of less than 4. At the same time, because of the limitation of sight at the roof of the Rutherford Physics Building, the altitude of the star during observing time needs to be larger than 30 degrees (ideally 45 degrees to be over all the blocking buildings), but it depends on the azimuth as well since not all directions are blocked. Since the time of the year and location on Earth have significant effects on the visibility of stars, the eclipsing stars list is obtained from the Observer's Handbook [8], and the astronomical object visibility plotter webpage airmass.org was used to obtain the available observing time for a certain star. An image of the available observing times of Algol and Capella is shown in Fig.4). After the search, only Algol satisfies most of the limitations. Algol is also called Beta Persei, and its magnitude is changing from 2.1 and regularly dips to 3.4 for each period.

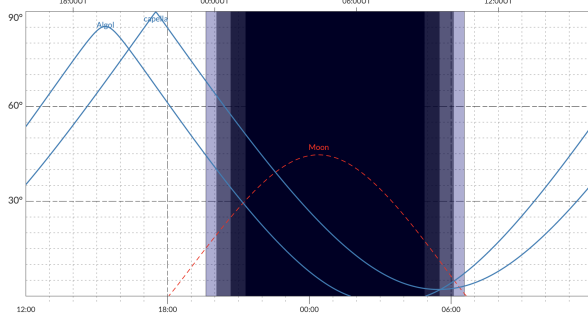


Figure 4: Altitude curves of Algol and Capella This is a daily chart on April 4, 2023, with the altitude of the star versus time. The sky starts to get dark around 7:30 pm, and it is completely dark after 9:00 pm. Algol rises and falls before Capella, which makes Capella able to be observed after taking the images with Algol.

The dark region in Fig.4 shows the sunset time and when the sky starts to get dark. In this case, the sky starts to get dark approximately at 7:30 pm and becomes completely dark after 9:00 pm. Algol is at an altitude of 44.7 degrees around 7:30 pm and quickly falls to 28.2 degrees when the sky is completely dark. After taking the images with Algol, a reference star was needed, and Capella was chosen because its altitude was still large enough for observation and it is a well-studied system. For a more detailed discussion of Capella refer to Sec.3.1.

2.5 Aperture Photometry

Aperture Photometry is a way to reduce background noises when calculating the flux of a star from a CCD image. It needs to locate the center of the star of interest, sum up the observed flux within the radius of the star of interest (the region within the radius should cover most of the fluxes from the star), and then subtract the summation of flux in the annular region with the same center, but with an inner radius larger than the previously stated radius, and an even larger outer radius. This is achieved by sequentially calling two custom functions.

First, `im_segmentation()` takes an RGB image as input and performs image segmentation to identify individual objects in the image. It first converts the image to grayscale and computes the threshold value for object detection using Otsu’s method. Otsu’s thresholding method is a way to automatically find a good threshold for separating an image into the foreground (what you want to detect) and background (what you don’t want to detect) [9]. It’s based on finding the threshold value that minimizes

the variance within each of these regions. This is done by analyzing the histogram of pixel intensities in the image. The result is a binary image where the objects are separated from the background. The properties of the detected objects, including their centroid, orientation, and axis lengths, are extracted using the `regionprops_table()` function from scikit-image and stored in a pandas dataframe.

Then, `RBP_flux()` takes the brightness data of an image and the segmentation output from `im_segmentation()` as inputs, and performs ring background photometry to measure the flux of a star in the image. It first defines a circular aperture with a radius equal to the average of the segmented star’s major and minor axis lengths. It then extracts the pixel values within this aperture and computes the total flux within the aperture. To compute the mean background level, the function defines an annulus around the star with inner and outer radii that are 5 and 10 pixels larger than the aperture radius, respectively. It then extracts the pixel values within this annulus and computes the mean background level. Finally, it subtracts the mean background level from the total flux to compute the background-subtracted flux. The function returns this background-subtracted flux.

3 Results

3.1 Capella Study

Capella (Alpha Aurigae) was our chosen reference star for this project. The theoretical luminosity of Capella is $(3.01 \pm 0.16) \times 10^{28}$ W [10] and the experimental luminosity was $(6.3 \pm 0.8) \times 10^{41}$ W. As expected, the discrepancy is non-negligible. However, this was the purpose of this part of the experiment. Capella was used to help calibrate and to introduce a scaling factor that would account for the difference between our experimental setup and the ones used in other peer-reviewed work. We determined the scaling factor to be $(4.8 \pm 0.7) \times 10^{-14}$. This means that if we scale by the same factor for Algol’s experimental data, the theoretical and experimental measurements should be comparable (within an order of magnitude). Comparing the experimental Capella data to the theoretical Capella data allowed us to determine the scaling factor needed to correct for any systematic differences between the two data sets. The theoretical Capella data we used here was the primary star’s luminosity in Capella. This was because the primary star had a luminosity of $78.7 \times L_{\text{sun}}$ [10] and the secondary star had

	Theoretical luminosity (W)	Experimental luminosity (W)	Scaled Experimental (W)
Capella	$(3.01 \pm 0.16) \times 10^{28}$	$(6.3 \pm 0.8) \times 10^{41}$	$(3.01 \pm 0.16) \times 10^{28}$
Initial Algol	$(6.97 \pm 0.08) \times 10^{28}$	$(1.25 \pm 0.24) \times 10^{42}$	$(6.0 \pm 1.4) \times 10^{28}$
Final Algol	$(6.97 \pm 0.08) \times 10^{28}$	$(1.26 \pm 0.16) \times 10^{42}$	$(6.0 \pm 1.1) \times 10^{28}$

Table 1: **Comparing Luminosities.** A comparison of the luminosities for Capella and Algol. The theoretical luminosity is the literature values that were found for each binary system, the experimental luminosity is the one we recorded with our observations, and the scaled experimental luminosity is the found value of luminosity after including a correction. The correction was determined by the initial analysis of Capella, and a scaling factor was determined of $(4.8 \pm 0.7) \times 10^{-14}$. The “Initial Algol” experimental values were before accounting for outliers, and the “Final Algol” experimental values were after outliers were eliminated using Moving Average interpolation. Note that the scaled experimental luminosity of Capella is the same as its corresponding theoretical value because the scaling factor was obtained from its experimental to theoretical results.

$72.2 \times L_{\text{sun}}$ [10], where L_{sun} was the luminosity of the sun which is 3.846×10^{26} W[11]. The luminosities of the two stars were close to each other, and they were eclipsing each other for most of the observation, meaning that one of the stars was blocking the other star for most of the time. Since the secondary star had a smaller radius than the primary star, it could not block the fluxes from the primary star completely. In either case of the eclipsing stage (primary eclipse or secondary eclipse), the primary star luminosity would contribute the most. We know that Capella is a well-studied binary system with a constant luminosity, which means that any variability observed in the experimental data is likely due to instrumental or environmental effects rather than intrinsic variability in the star. These differences can then be corrected by applying a scaling factor to the experimental Algol data. This approach is valid as long as we can assume that the instrumental and environmental effects affecting Capella are the same as those affecting Algol. We used the same instruments to record our data for both star systems (see Fig.3), and took our measurements at the same location on the same night. However, there may be some differences in the instrumental and environmental effects between Capella and Algol that are unaccounted for. Additionally, if there are any intrinsic variations in Capella that we are not aware of, these could also affect the scaling factor. Therefore, it is important to carefully consider the assumptions underlying this approach and to validate the results using other methods if possible.

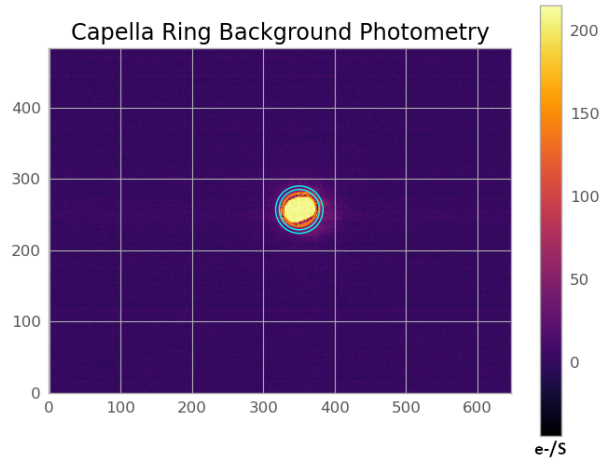


Figure 5: Aperture Photometry for Capella Ring background photometry of Capella at the time (April 4, 2023, 9:44 pm) with a radius difference of 5 between inner and outer radius annulus with a colour bar ranging from 0 to $200 \text{ e}^{-\text{s}}^{-1}$. The orange circle represents the aperture radius used for photometry, and the teal blue circle represents the inner and outer annulus used for background subtraction. Ring background photometry is a technique used to accurately measure the flux of an object while minimizing the contribution of background sources.

3.2 β Persei Study

Our initial experimental data values for Algol using the scaling factor are shown in Table 1 as “Initial Algol”. Due to systematic errors, some data points were visually worse than others (see good image versus bad image comparison in Appendix B.1). Some sources of systematic error include moving the telescope during data collection (shifting weight on the platform or wind), light pollution in the city, and the different altitudes of the two binary systems. These visually distorted data points correspond to flux data points that initially appeared like outliers

on the light curve plot. We used the descriptive statistical method of the Inter-Quartile Range (IQR) to measure the variability in a data set. It is the difference between the upper and lower quartiles of the data, and represents the spread of the middle 50 percent of the data points.) Using the quartiles as “fences” for our dataset, we can find the outlier values. The IQR method identified the following images as outliers: 15, 16, 129, 142, and 143. To replace these outliers, the method of Moving Average (MA) interpolation was used. Given that images 142 and 143 were the last two measurements, they are simply ignored in the following steps of the analysis. MA suggested replacing the remaining outliers with 1.2×10^5 , 1.1×10^5 , and $1.1 \times 10^5 e^{-s^{-1}}$ respectively. The resulting light curve can be observed in Fig.6 all the while the light curve including outliers can be found in Appendix B.2.

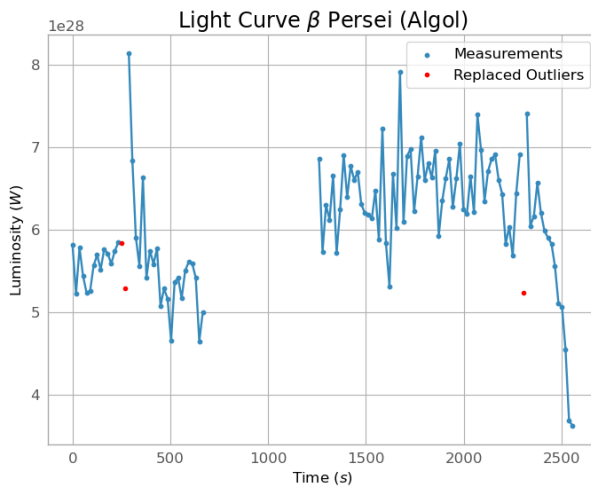


Figure 6: Experimental Light Curve of Algol with Scaled Luminosity and Interpolated Outliers The experimental luminosity values (blue) were scaled by a factor of $(4.8 \pm 0.7) \times 10^{-14}$ to match the mean theoretical luminosity [12]. The observed gap in the data is due to the two separate runs of measurements. Outliers were identified using IQR and then replaced using the method of moving average interpolation, shown in red.

The resulting luminosity is shown in Table 1 as “Final Algol”. Comparing the initial version of Algol data to the final, we can see that the latter is more precise (with an error of 1.1 vs 1.4) and keeps the same accuracy (rounded to 6.0) in both cases.

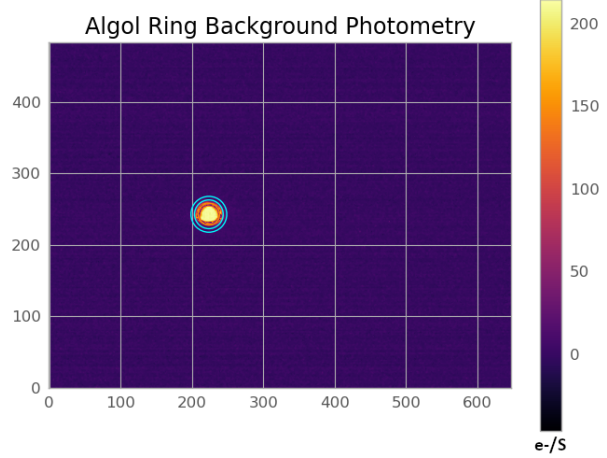


Figure 7: Aperture Photometry for Algol Ring background photometry of Algol at the time (April 4, 2023, 8:53 pm) with a radius difference of 5 between inner and outer radius annulus with a colour bar ranging from 0 to $200 e^{-s^{-1}}$. The orange circle represents the aperture radius used for photometry, and the teal blue circle represents the inner and outer annulus used for background subtraction. Ring background photometry is a technique used to accurately measure the flux of an object while minimizing the contribution of background sources.

3.3 Light Curve Study

The theoretical data was obtained from the TESS database from the 2022 mission. This was the most recent data we could find. We originally tried a TESS dataset from 2019, however, the precision of the measurements was too large to be comparable to our dataset. Therefore, we went with the 2022 dataset, but the 2019 plot can still be seen in Appendix B.2, which shows the periodic behaviour of Algol’s light curve. The data was recorded with CCD measurements as well, so it also needed to scale to Algol’s actual luminosity. We fitted the maximum value in TESS data to Algol’s primary star luminosity $182 \times L_{\text{sun}}$ [13], where L_{sun} was $3.846 \times 10^{26} \text{ W}$ [11], and it gave Algol primary’s luminosity $7.00 \times 10^{28} \text{ W}$. We chose to fit the primary star’s luminosity because the secondary star had a theoretical luminosity $6.92 \times L_{\text{sun}}$ [13], and it would only affect the total luminosity of Algol by 3.8%. The period of eclipsing was 2.87 days. The plot in Fig.8 showed the first eclipsing period of TESS data, and the red region was where our data would be if we shifted our data horizontally by complete periods. The position of our first data was 189970.30 s after the initial point of TESS’s data, or in other words, the phase change was 189970.30 s, and we were in the time region where the binary stars are not eclips-

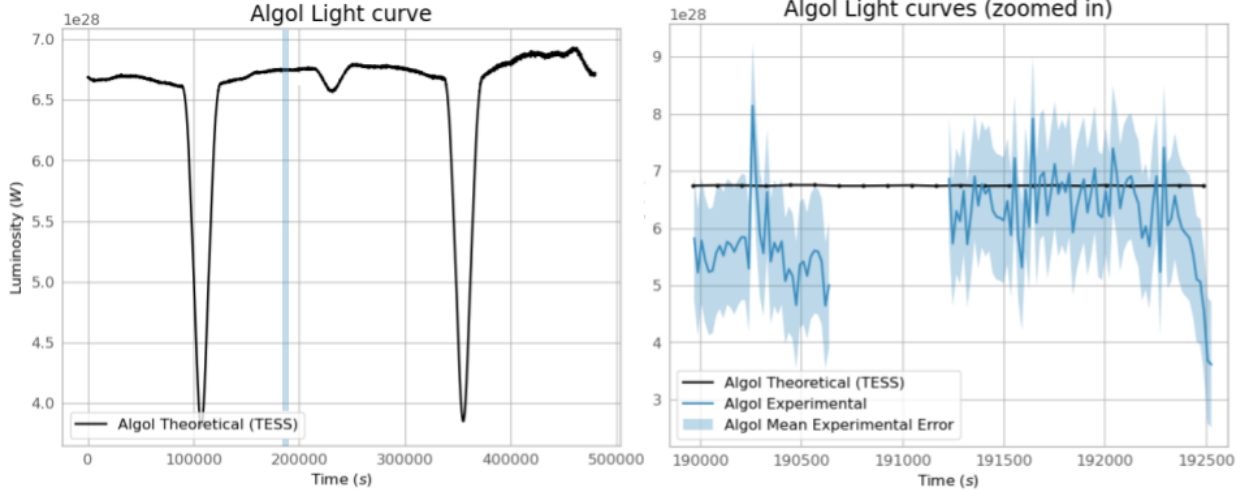


Figure 8: Algol light curve comparison On the left, in black, is the full first period of Algol from the TESS mission. We plot the luminosity (in W) vs time (in s). In blue is highlighted the region of interest. On the right, we zoom in on the region of interest. In black, we still have the data collected by the TESS mission, and in blue, we have the data we collected (our experimental data of Algol). In light blue is the mean error of the experimental data (in W). The expected values for 69.4% of the points fall within the error bars.

ing each other. This means that the theoretical data (i.e. TESS’ measurements) corresponding to our measurements are constant and follow the flat part of Algol’s light curve. The next time duration would be a secondary eclipse.

Throughout our region of interest, a theoretical mean of 6.8×10^{28} W was observed with TESS data. As it did with the data obtained by *Baron et al.* [12]; it falls within one standard deviation of our calculated mean. When comparing our measured mean luminosity and TESS’ mean luminosity, one can calculate a percent error of 11.8%. Moreover, when considering the average luminosity error, Fig.8 shows that the expected values for 69.4% of the points fall within the error bars.

4 Discussion

There were several potential systematic errors in doing our observations of Capella and Algol. The biggest systematic error was that the two stars were at different altitudes in the night sky. Algol dropped in altitude very fast and it went below 30 degrees for the most observing time. The stars at the same altitude were either blocked by the surrounding buildings or were not bright enough to observe. Because the two stars are at different elevations, the starlight goes through different atmospheric conditions. The *airmass* is defined as the amount of air along the

line of sight when observing a celestial source from below Earth’s atmosphere [14]. Algol has an altitude of 32.2 degrees at the 8:53 pm observing time, and an altitude of 25.8 degrees at the 9:36 pm observing time. Capella has an altitude of 46.6 degrees at the 9:47 pm observing time. The airmass of Algol was 1.88 atm and 2.29 atm (respectively), while Capella’s airmass was 1.38 atm. These numbers were calculated using the airmass.org website, which allowed us to input our time of observation, location of our observatory, and our right ascension and declination values for each star as recorded by our *Celestron C8* telescope. This means that Algol’s starlight experiences far more distortion in the atmosphere than Capella. This atmospheric distortion will induce the dimming of Algol’s light. If two binary star systems were closer in altitude and fulfilled the requirements we needed for observations at the Anna McPherson Observatory (a minimum apparent magnitude of 4), those would have been chosen instead. However, if the observing data was divided into two sections, one before the gap and one after the gap, the second part of the data had a higher luminosity than the first part. As discussed above, the airmass was increasing for Algol as time passed, we should expect the luminosity of Algol to be lower in the second part.

The gap appeared because Algol moved out of the region of the CCD camera and the image of Algol needed to be re-centered. The location of the telescope did not move, but the pointing direction

moved about 2 degrees in both altitude and azimuth. This was also obtained from airmass.org website as the time of the last data point on the first part and the time of the first data point on the second part could be located on the Fig.4, and the website could show the associated position of the star. Since the ring background photometry was applied to the data, the reason why there was an increase between the two parts should not be the difference in the light pollution at different pointing directions. This could be due to the self-heating of the CCD camera, as it could have a significant temperature increase when it was working. When there was a 10 min gap between the two parts, the CCD camera was not operating and cooled down. The dark frames were taken one between the measurements of Algol and Capella and the other after the measurements of Capella, as the observation of Algol was time-consuming (as discussed in Sec.2.4, the best observing time for Algol was before the sunset, and after the sky is completely dark, Algol's altitude dropped quickly). It was also because the exterior temperature dropped fast when the sky gets dark, which would make the dark frame meaningless if it was taken before complete darkness. The dark frame taken between the measurements of the two stars had a mean value of 42.82 and the other one had 43.99. The changes were not significantly large, but it could be due to the self-heating of the CCD camera. And if this is the reason, and given that the time between taking the two dark frames was much shorter than 10 minutes, it could lead to the result of the increase between the two parts.

Some other systematic sources of error include moving the telescope during observation by people shifting weight on the observation platform or wind. The telescope was incredibly sensitive to ground vibrations and we tried to stay as still as possible during observation, but we cannot guarantee that there were no ground vibrations during data collection.

The plot shown in Fig.8 shows the light curve of Algol from the theoretical TESS values and our experimental values. The theoretical light curve is much flatter than our experimental values. Since TESS is an orbiting satellite, it does not have to deal with atmospheric conditions when collecting data and thus results in a much smoother dataset. The second part of our experimental light curve is much closer in approximation to the theoretical light curve than our initial recording. In the Results section, we found that our precision error between the experimental luminosity and TESS' mean luminosity is 11.8%. The precision is a bit high (most

precision values are between 5 – 10% [15]), but as mentioned, a large part of this difference is likely due to atmospheric conditions. However, other statistical methods show that our data is good despite the precision error. Using the 2/3 rule [16], about 69.4% of our error bars on our experimental light curve fall within the theoretical light curve. In addition, Table 1 showed that our scaled experimental luminosity value for Algol was within one standard deviation of the experimental luminosity value from TESS. The light curve observed is during the transit duration phase, which was expected given the period of Algol (~ 2.8 days) and the date of our observation. Thus the relative flatness of the plot is to be expected.

To get a better approximation of Algol's expected light curve, the following tasks could be done in a future experiment. More dark frames could be taken between measurements to better understand the temperature fluctuation bias throughout the night and how CCD camera noise is affected by temperature (in a quantitative sense). A longer period of observation, possibly over several weeks could be done to get a more accurate shape of Algol's light curve, and not just a singular component of the period, like in this experiment. As discussed earlier, choosing a reference star at the same altitude as an interest star would mitigate the effects of air mass and atmospheric conditions on our observations. However, due to the light pollution in Montreal only allowing star observations of at least apparent magnitude 4, our options were much more limited. In a more remote observing location, two reference stars at close altitudes would be more feasible.

5 Conclusion

In this project, we aimed to reproduce the light curve of the Beta Persei binary star system from the Transiting Exoplanet Survey Satellite (TESS) mission using our experimental data. Our experimental light curve of Algol was largely consistent with the theoretical light curve, with 69.4% of error bars falling within the theoretical light curve. The precision error between experimental and theoretical luminosity was high (11.8%) and likely due to atmospheric conditions. However, our data is still good despite the precision error, for our scaled experimental luminosity ($(6.0 \pm 1.1) \times 10^{28}$ Watts) was within one standard deviation of the TESS data ($(6.97 \pm 0.08) \times 10^{28}$ Watts). Some sources of error in this experiment included the differing air masses and atmospheric conditions of Algol and Capella's observations, a 10-

minute gap between our observations, potential temperature fluctuation bias in the CCD camera, and the telescope's sensitivity to ground vibrations. Despite the error, we achieved our goal of observing and recording the light curve of Algol, with our experimental data showing consistency with the theoretical light curve. In a future experiment, we would aim to take more dark frame measurements, conduct a longer period of observation of Algol's light curve, and choose a different observing location to utilize two reference stars of the same altitude.

Acknowledgement

We would like to thank Samantha Wong for her support and guidance throughout this enterprise. Additionally, we would like to express our gratitude to Matthew Lundy for his help setting up and calibrating the telescope as well as for his help on the analysis pipeline of this report.

References

- [1] R. W. Hilditch. *An Introduction to Close Binary Stars*. Cambridge University Press, 2001. ISBN: 9781139163576.
- [2] David A. Aguilar. *Most Milky Way Stars Are Single*. URL: <https://pweb.cfa.harvard.edu/news/most-milky-way-stars-are-single>.
- [3] Joseph Henry Press. “FLUX, LUMINOSITY AND THE INVERSE SQUARE LAW”. In: *One Universe: Energy Knowledge Concept* 7 (2015). URL: https://nap.nationalacademies.org/jhp/oneuniverse/energy_knowledge_concept_7.html.
- [4] *oaCapture 1.5.0. User Manual*. 2020. URL: <https://www.openastropoint.org/documentation/oacapture-1-5-0-user-manual/>.
- [5] *Neximage 5 Solar System Imager (5MP)*. 2023. URL: <https://www.celestron.com/products/neximage-5-solar-system-imager-5mp#description>.
- [6] Jonathan St-Antoine. *Advanced CCD Techniques*. Starizona, 2004.
- [7] LLC. Celestron. *Nexstar 8se Computerized Telescope*. 2023. URL: <https://www.celestron.com/products/nexstar-8se-computerized-telescope#description>.
- [8] James S. Edgar, ed. The Royal Astronomical Society of Canada, 2023. ISBN: 978-1-927879-30-6.
- [9] Anastasia Murzova and Sakshi Seth. “Otsu’s Thresholding Technique”. In: *LearnOpenCV* (May 2021). URL: <https://learnopencv.com/otsu-thresholding-with-opencv/>.
- [10] Guillermo Torres et al. “Capella (aurigae) revisited: New binary orbit, physical properties, and Evolutionary State”. In: *The Astrophysical Journal* 807.1 (2015), p. 26. DOI: 10.1088/0004-637x/807/1/26.
- [11] The Astropy Developers. *Constants (astropy.constants)*. URL: <https://hेत.utsexas.edu/HET/Software/Astropy-1.0/constants/index.html>.
- [12] F. Baron et. al. “Imaging the Algol Triple System in the H band with the CHARA interferometer”. In: *The Astrophysical Journal* 752.1 (May 2012), p. 20. DOI: 10.1088/0004-637x/752/1/20. URL: <https://doi.org/10.1088/0004-637x/752/1/20>.
- [13] S. Soderhjelm. “Geometry and dynamics of the Algol system”. In: 89.1-2 (Sept. 1980), pp. 100–112.
- [14] Daniel W. E. Green. “Correcting for Atmospheric Extinction”. In: *International Comet Quarterly* 14 (July 1992), pp. 55–59. URL: <http://www.icq.eps.harvard.edu/ICQExtinct.html>.
- [15] Rapid Sigma Solutions LLP. “Is my measured data acceptable?” In: *Analytics, Lean, Six Sigma, and Project Management Analysis Software* (2023). URL: <https://www.sigmapmagic.com/blogs/is-my-measured-data-acceptable/>.
- [16] Erik W. Grafarend. De Gruyter, 2006.
- [17] “TESS Planet Count and Papers”. In: *TESS Transiting Exoplanet Survey Satellite* (2019). URL: <https://tess.mit.edu/publications/>.

A Appendix (Python Scripts)

For complete scripts, plots and project architecture please refer to the project repository.

B Appendix (Additional Figures)

B.1 Calibration and Data

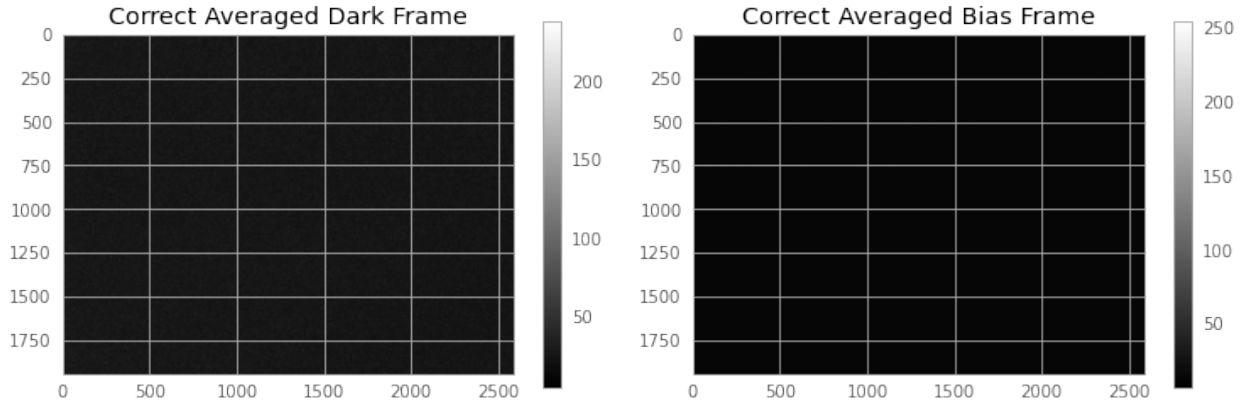


Figure 9: Mock Calibration Frames The Mock Calibration frames were taken to familiarize ourselves with the CCD camera. The left plot is the averaged Dark Frame, and the right plot is the averaged Bias Frame.

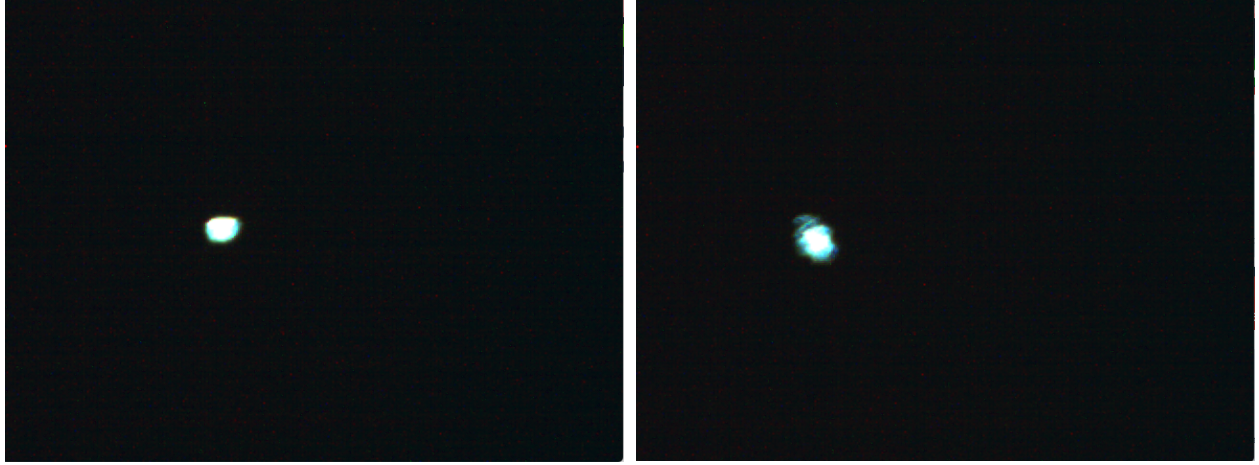


Figure 10: Good vs Bad Algol Images A comparison of good versus bad astrophotography for Algol images. As they were discussed in the results, a source of systematic error can include moving the telescope during data collection, or by vibrations on the observing floor. This systematic error is very obvious in these two photographs. The left picture is a clear image of Algol, with little aberration. The right picture is an unusable picture of Algol, for the aberration on the image will result in a variable dataset. The aberration in the image is likely due to some movement that occurred around the telescope when this picture was taken.

B.2 Light Curves

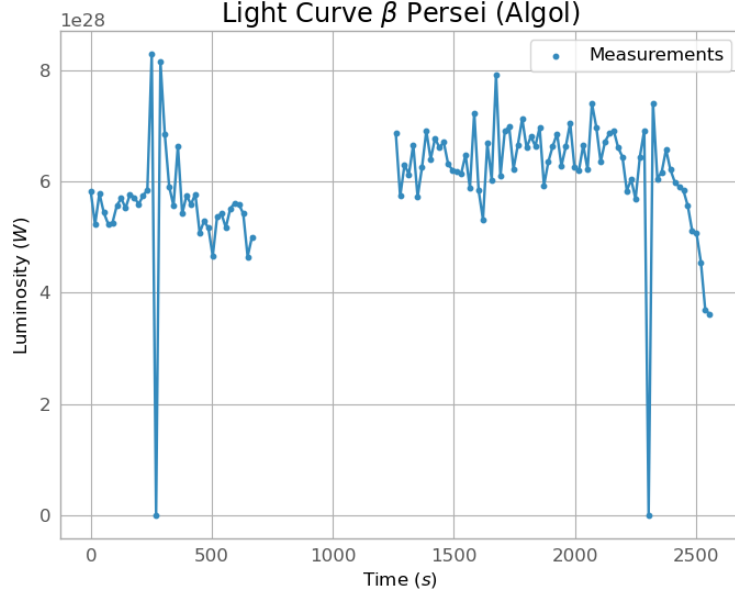


Figure 11: Experimental light curve of Algol showing the transit duration phase The data points in blue are the original measurements, including outliers. The data has been scaled by a factor of $(4.8 \pm 0.7) \times 10^{-14}$ to match the theoretical data using Capella as a reference star. There is a horizontal gap because measurements were made in two runs.

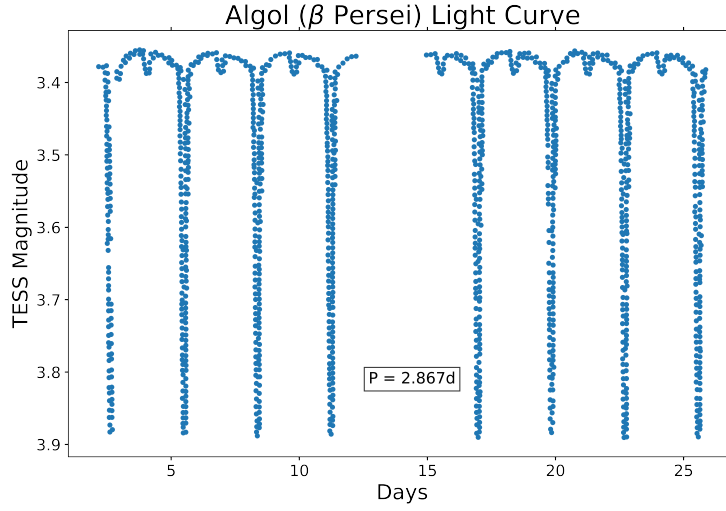


Figure 12: TESS Data of Algol Light Curve This plot is an example of the theoretical data for the light curve of Algol measured with NASA's Transiting Exoplanet Survey Satellite (TESS). The light curve of Algol has an orbital period of ~ 2.8 days, which is the time between recorded primary dips in the light curve. The secondary eclipse of the binary system is shown by the secondary dips in the light curve. We did not end up using this theoretical dataset, as the precision between measurements was too large. We chose a different dataset to compare the two, which is shown in the main text. However, we chose to include this plot as well because it shows the regular periodicity of Algol's light curve [17].